ISSN 0023-1584, Kinetics and Catalysis, 2011, Vol. 52, No. 3, pp. 446–458. © Pleiades Publishing, Ltd., 2011.
Original Russian Text © A.S. Ivanova, E.V. Korneeva, G.A. Bukhtiyarova, A.L. Nuzhdin, A.A. Budneva, I.P. Prosvirin, V.I. Zaikovskii, A.S. Noskov, 2011, published in Kinetika i Kataliz, 2011, Vol. 52, No. 3, pp. 457–469.

Hydrocracking of Vacuum Gas Oil in the Presence of Supported Nickel–Tungsten Catalysts

A. S. Ivanova, E. V. Korneeva, G. A. Bukhtiyarova, A. L. Nuzhdin, A. A. Budneva, I. P. Prosvirin, V. I. Zaikovskii, and A. S. Noskov

Boreskov Institute of Catalysis, Siberian Branch, Russian Academy of Sciences, Novosibirsk, 630090 Russia

e-mail: iva@catalysis.ru

Received July 12, 2010

Abstract—The supports containing 70% Al_2O_3 and 30% β zeolite (AZ-1 and AZ-2), which differed in mixing procedures, and the Ni–W/AZ-1 and Ni–W/AZ-2 catalysts were characterized using an adsorption technique, high-resolution electron microscopy, IR spectroscopy, and X-ray photoelectron spectroscopy and tested in the hydrocracking reaction of vacuum gas oil (VGO). It was found that the supports differed in texture characteristics and surface Lewis acidity at the same composition and similar concentrations of Brønsted acid sites. The formation of Ni–W–S sulfide species on the surfaces of both of the supports occurred in different manners: multilayer Ni–W–S sulfide species were formed on AZ-1 (S_{sp} = 220 m^2/g), whereas single-layer species were mainly formed on AZ-2 (S_{sp} = 380 m^2/g). It was found that catalysts containing multilayer Ni–W–S sulfide species, which were characterized by a higher degree of sulfidation, provided a higher yield of diesel fuel upon the hydrocracking of VGO, whereas catalysts containing single-layer Ni–W–S sulfide species were more active in the reactions of VGO hydrodesulfurization and hydrodenitration.

DOI: 10.1134/S0023158411030098

INTRODUCTION

In recent years, the following tendencies are observed in the world petroleum refining industry:

—the involvement of heavier petroleum fractions containing large amounts of heteroatomic impurities in processing;

—an increase in the depth of petroleum refining for increasing the yield of light oils, which is related to an increase in the relative fraction of destructive processes;

—strict environmental regulations imposed on the quality of fuels with necessary deep purification and refinement.

By 2015, the depth of petroleum refining in the Russian Federation should be 80%. In this case, the production of petroleum residue should be decreased [1] because of its vacuum distillation to obtain light oil—vacuum gas oil (VGO). With the use of currently available technologies, the fraction of VGO can reach 70%. The necessity of increasing the degree of conversion of heavy petroleum fractions into light motor fuels stimulated the more widespread introduction of VGO hydrofining and hydrocracking processes, which are performed at elevated temperatures and hydrogen pressures with the use of different catalysts under different conditions with different distributions of the reaction products [2]. VGO usually contains to 3 wt % sulfur [3, 4]. According to Eijsbouts et al. [5], a decrease in the sulfur content of VGO to 450 or 190 ppm makes it possible to obtain gasoline containing less 25 or 10 ppm of sulfur, respectively.

The VGO hydrofining and hydrocracking processes are performed in a fixed bed of a catalyst in a three-phase reactor (gas–liquid–solid catalyst). Gaseous hydrogen contacts liquid VGO under process conditions; it passes through the reactor filled with catalyst granules from top to bottom. Hydrogen pressures from 8 to 20 MPa at 360–440°C are used in the hydrocracking of VGO. Along with the removal of sulfur, nitrogen, oxygen, and metals, the production of motor fuel (gasoline and/or diesel fuel) is the main goal of the hydrocracking of VGO.

Hydrocracking reactions also occur in VGO hydrofining reactors; however, in this case, the conversion of a heavy fraction is no higher than 10%. At a conversion of 10–50%, the case in point is the process of light (mild) hydrocracking; in the case of deep hydrocracking, the conversion is higher than 50% [3]. In this context, conversion is the fraction of a raw material transformed into light petroleum products (gasoline, kerosene, and diesel fuel); the unconverted residue is a fraction whose boiling point is higher than 360°C for VGO.

The process efficiency of the hydrocracking of VGO depends on the nature of the utilized catalyst, which, in turn, should be bifunctional: it should be active in hydrogenation–dehydrogenation reactions on the one hand and in cracking reactions on the other

hand. Metals are responsible for the activity in hydrogenation–dehydrogenation reactions, whereas the activity in cracking reactions is due to the presence of acid sites in the supports. The commonly used supports are amorphous oxides such as aluminosilicates [6], crystalline zeolite in combination with aluminum oxide, or a mixture of crystalline zeolite with amorphous oxides. Bataille et al. [7] assume that β zeolite is the most suitable acidic component for the hydrocracking of gas oil because it possesses specific acidity and suitable pore structure. Attention has been focused on this zeolite because of its high Si : Al ratio, activity in hydroisomerization, enhanced stability to deactivation, and accessibility to the use in petrochemical processing [8, 9]. The metals responsible for the hydrogenating–dehydrogenating function are mainly Group VIA (molybdenum and tungsten) and Group VIIIA (cobalt and nickel) metals of the periodic table. It should be noted that an optimum ratio between the above catalyst functions is necessary for obtaining an active and selective catalyst for the hydrocracking of VGO [10]. Accordingly, the development of highly effective catalysts for the hydrofining and hydrocracking of VGO is of considerable current interest.

This work was devoted to study the effects of procedures used for preparing a support (Al_2O_3 + zeolite) and supporting an active component (Ni–W) on it upon the texture and acidic properties of the supports and the distribution and surface properties of the active component and to determine a relation of these characteristics to the activity and selectivity of the resulting catalysts in the hydrocracking reaction of VGO.

EXPERIMENTAL

Preparation of Supports and Catalysts

Preparation of supports. For the preparation of the supports, aluminum oxide (γ-Al_2O_3: $S_{BET} \approx 300$ m^2/g; average pore diameter, 135 Å) and β zeolite in the H form (SiO_2 : Al_2O_3 = 25; $S_{BET} \approx 400$ m^2/g), whose characteristics were almost the same as those given in [10], were used as starting substances. Two supports containing 70% Al_2O_3 (**A**) and 30% β zeolite (**Z**) were prepared using different mixing procedures. Support AZ-1 was obtained by the mixing of aluminum oxide and zeolite in the presence of a solution of phosphoric acid with the acid modulus $M = 0.1$; support AZ-2 was prepared by the mixing of zeolite, aluminum oxide, and aluminum hydroxide, which was used as a binding agent. The synthesized supports were dried at 110°C for 12–14 h and then calcined at 550°C for 2–2.5 h.

Preparation of catalysts. The catalysts were obtained by (a) the incipient wetness impregnation of a support (cylindrical granules 1.5 mm in diameter and 4–6 mm in length) using a mixed solution of corresponding salts, ammonium metatungstate ($(NH_4)_6H_2W_{12}O_{39} \cdot 5H_2O$) and nickel nitrate ($Ni(NO_3)_2 \cdot 4H_2O$); (b) the sequential incipient wetness impregnation of a support initially with a solution of ammonium metatungstate and then with a solution of nickel nitrate with intermediate drying at 110°C for 12 h; or (a*) the impregnation with a mixed solution of the above salts in the presence of a complex-forming agent (citric acid). Then, the samples were dried at 110°C for 12 h and calcined at 500°C for 2 h in a flow of either air or nitrogen. The catalysts were designated as follows: Ni–W/AZ-1(a), Ni–W/AZ-1(b), Ni–W/AZ-2(a), and Ni–W/AZ-2(a*). The concentrations (wt %) of supported active components in the catalysts were (3.6 ± 0.2) for NiO and (15.6 ± 0.2) for WO_3. The resulting oxide catalyst precursors were sulfidized in accordance with the procedure described in the Catalytic Activity Determination section.

Support and Catalyst Characterization Methods

Texture characteristics. The texture characteristics of the supports were determined on an ASAP-2400 instrument (Micromeritics) from the isotherms of low-temperature (–196°C) nitrogen adsorption; the samples were preliminarily kept in a vacuum at 150°C for 16–18 h; the error of the method was ±10%.

Acid properties. The acid properties of the supports were investigated by the IR spectroscopy of adsorbed CO, which forms complexes with Lewis acid sites (LASs) and Brønsted acid sites (BASs). An increase in the vibration frequency of adsorbed CO with respect to the value for the molecule in a gas phase ($\nu(CO) = 2143$ cm^{-1}) was caused by the formation of complexes with LASs. The shift of the band ν(CO) to the region of high frequencies characterizes the strength of LASs because it is related to the heat of formation of the complexes by the function $Q_{CO} = 10.5 + 0.5(\nu(CO) - 2143)$. The concentration of LASs was measured from the integrated intensity of absorption bands due to adsorbed CO (in the spectral region of 2185–2240 cm^{-1}) according to the formula N [μmol/g] $= A/A_0$, where A is the integrated intensity of a band due to adsorbed CO, and A_0 is the integral absorption coefficient [11].

For measuring the spectra, the samples were pressed as pellets with a density of $(10–20) \times 10^{-3}$ g/cm^2 without the binding agent. Before the adsorption, the sample was heated in a vacuum at 500°C for 2 h. The adsorption of CO was performed at –196°C over a pressure range of 0.1–10 Torr. The IR spectra were recorded on a FTIR-8300 Fourier transform spectrometer (Shimadzu) with a resolution of 4 cm^{-1}; 100 scans were accumulated for each spectrum. The IR spectra were normalized to the pellet density; the accuracy of the concentration measurements was ±15%.

Main component concentrations. The concentrations of the main components were determined by atomic absorption spectrometry [12].

Electron-microscopic studies. The electron-microscopic studies of the samples were conducted on a JEM-2010 transmission electron microscope (JEOL) (resolution, 0.14 nm; accelerating voltage, 200 kV). Local energy-dispersive x-ray analysis (EDX), which was carried out on an EDAX spectrometer (EDAX Co), was used for determining the concentrations of elements and ratios between them. The test samples were supported onto a carbon substrate immobilized on copper gauze.

X-ray photoelectron spectra. The X-ray photoelectron spectra of samples Ni–W/AZ were obtained on a photoelectron spectrometer (SPECS) equipped with a PHOIBOS-150 hemispherical analyzer and an XR-50M source of characteristic X-rays with a double Al/Ag anode and a FOCUS-500 X-ray monochromator. Monochromated AlK_α radiation ($h\nu = 1486.6$ eV) was used for recording the spectra. The scale of binding energies (E_B) was precalibrated using the peak positions of the gold and copper core levels Au $4f_{7/2}$ (84.0 eV) and Cu $2p_{3/2}$ (932.67 eV). The samples were supported onto bilateral conducting copper Scotch tape. The C1*s* line (284.8 eV) from carbon, which was present on the catalyst surface, was used for calibration. Survey spectra were written at a transmission energy of 50 eV; individual sections were written at 20 eV. The relative concentrations of elements on the catalyst surfaces and the ratios between their atomic concentrations were determined from the integrated intensities of photoelectron lines corrected for the appropriate atomic sensitivity coefficients [13].

Catalystic Activity Determination

Catalyst activity in the reaction of VGO hydrocracking was determined on a pilot plant containing two identical reactors with an inside diameter of 26 mm and a length of 1300 mm. VGO from a heated reservoir, which was arranged on an electronic balance for automatically controlling the feed rate, was supplied using Gilson-305 liquid chromatographic pumps equipped with thermostatically controlled devices. Hydrogen was supplied with a Bronkhorst automated flow controller; the feed and hydrogen entered the reactor from top to bottom. The reactors were placed in tube furnaces with three independent heating zones, which ensured the occurrence of an isothermal zone at the central section of the reactor. Testing was performed with the use of catalyst granules as cylinders 1.5 mm in diameter and 4–6 mm in length. A specified catalyst volume (20 cm^3) was placed in the isothermal reactor zone and diluted with silicon carbide particles of size 0.1–0.2 mm in a volume ratio of 1 : 2. The bed of the diluted catalyst was arranged between two layers of silicon carbide (particle diameter of 3–4 mm); the temperature in the catalyst bed was controlled with a five-point mini thermocouple, which was mounted vertically at the central section of the reactor.

The catalyst was dried at 140°C for 4 h in a flow of hydrogen; then, it was moistened with a straight-run diesel fraction and sulfurized with the use of a straight-run diesel fraction, which additionally contained 1 wt % sulfur as dimethyl disulfide. The space velocity of a mixture for sulfidation was 2 h^{-1}, and the hydrogen to raw material ratio was 500. The sulfidation was performed stepwise: at 240°C for 6 h, at 340°C for 4 h, and at 360°C for 4 h. The rate of heating was no higher than 25 K/h. A light diesel fraction with the final boiling temperature of 340°C was used for moistening the catalyst and preparing a sulfidizing mixture.

After the completion of the sulfidation procedure, the pressure of hydrogen was increased to 10 MPa and VGO was supplied to the reactor in place of the diesel fraction. The catalysts were tested at a feed space velocity of 1 h^{-1}, a hydrogen to raw material ratio of 1000, and a pressure of 10 MPa in the temperature range of 380–410°C. VGO (340–540°C) with a specific density of 0.92 g/cm^3 and sulfur and nitrogen concentrations of 2.12 and 0.081 wt %, respectively, was used as the starting material.

The feed after the reactor entered a low-pressure separator, where it was separated into liquid and gas phases, and the liquid phase was blown with nitrogen for the removal of hydrogen sulfide and ammonia formed in the course of the reaction. For comparing the catalytic properties of catalysts, analysis was carried out to determine the fractional composition and the concentrations of sulfur and nitrogen in the resulting hydrogenation products.

For determining the total sulfur contents of VGO and its hydrofining products, a Lab-X 3500SCl energy-dispersive X-ray fluorescence analyzer. The trace amounts of nitrogen and sulfur in petroleum products were determined with the use of an ANTEK 9000NS sulfur/nitrogen analyzer in accordance with ASTM D 5762 and ASTM D 5453 standard procedures. The fractional composition of starting materials and hydrogenation products were determined by simulated distillation in accordance with an ASTM 2887 standardized procedure with the use of an Agilent 6890N chromatograph equipped with a DB-1 chromatographic capillary column (the length of 10 m, the inside diameter of 0.53 mm, and the film thickness of 2.65 μm) and the Chemstation SimDis software. The determination of the concentrations of aromatic compounds in the resulting diesel fuel was carried out in accordance with Institute of Petroleum standard method IP 391/395 (European Standard EN 12 916)

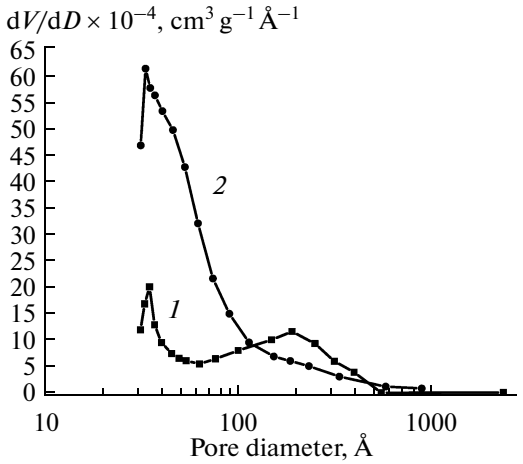

Fig. 1. Pore size distributions for supports (*1*) AZ-1 and (*2*) AZ-2.

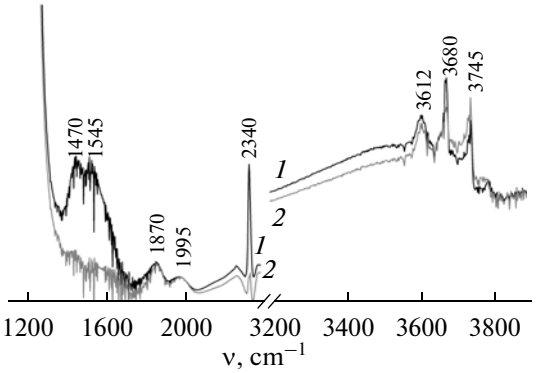

Fig. 2. IR spectra of supports (*1*) AZ-1 and (*2*) AZ-2 after evacuation at 500°C.

by liquid chromatography on a Varian ProStar chromatograph completed with a refractometric detector.

The conversion (X) of VGO, the selectivity (S), and the yields (Y) of various products were calculated from the equations

$$X = \frac{W_{GO} - W_R}{W_{GO}} \times 100, \quad S_i = \frac{W_i}{W_{GO} - W_R} \times 100,$$

$$Y_i = \frac{W_i}{W_{GO}} \times 100,$$

where W_{GO} is the weight of the starting material, W_R is the weight of the residue with true $T_b > 360$°C, and i is a fraction of the specified composition.

RESULTS AND DISCUSSION

Characteristics of the Supports

Texture characteristics of the supports. According to low-temperature nitrogen adsorption data (Fig. 1, Table 1), supports AZ-1 and AZ-2 are different in both pore-size distributions and texture characteristics. It can be seen (Table 1) that the preparation of support AZ-2 with the use of aluminum hydroxide as a binding agent resulted in an increase in the specific surface area by a factor of about 1.7 in comparison with AZ-1; in this case, the average pore diameter was 45 Å against 70 Å. At the same time, the pore volumes of the test supports differed insignificantly. It is believed that the dispersity of a Ni–W component on support AZ-2 is higher than that on support AZ-1.

Acid–base properties of the supports. Figure 2 shows the IR spectra of the supports after evacuation at 500°C. In the spectrum of support AZ-1, absorption bands at 1470–1545 and 2340 cm^{-1} indicate the presence of the carbonate ion CO_3^{2-} and CO_2, respectively [14, 15] (the latter was likely due to the encapsulation of CO_2 in closed pores); absorption bands at 1870 and 1995 cm^{-1} are the overtones characteristic of the zeolite framework. In the spectrum of support AZ-2, these structures did almost not occur. Hence, we can conclude that carbonate species were present on the surface of AZ-1 as a result of the procedure used for the preparation of parent aluminum oxide; therefore, they can lead to a decrease in its specific surface area.

Figure 2 shows the IR spectra of the supports in the region of hydroxyl groups, and Figure 3 shows their decomposition into individual components. It is evident that the above spectra contain ten absorption bands, of which an absorption band at 3580 cm^{-1} belongs to hydrogen-bonded OH groups. In this case, it is impossible to ascribe the other absorption bands to certain structural groups. However, it is most likely that a low-frequency absorption band at 3612 cm^{-1} belongs to the bridging OH groups of zeolite, and an absorption band at 3745 cm^{-1} is due to Si–OH groups

Table 1. Texture characteristics of the supports used for preparing catalysts for the hydrocracking of VGO

Catalyst	Support	S_{sp}, m^2/g	V_{pore}, cm^3/g	D_{pore} (average), Å
Ni–W/AZ-1(**a**) Ni–W/AZ-1(**b**)	AZ-1	220	0.5	70
Ni–W/AZ-2(**a**) Ni–W/AZ-2(**a***)	AZ-2	380	0.6	45

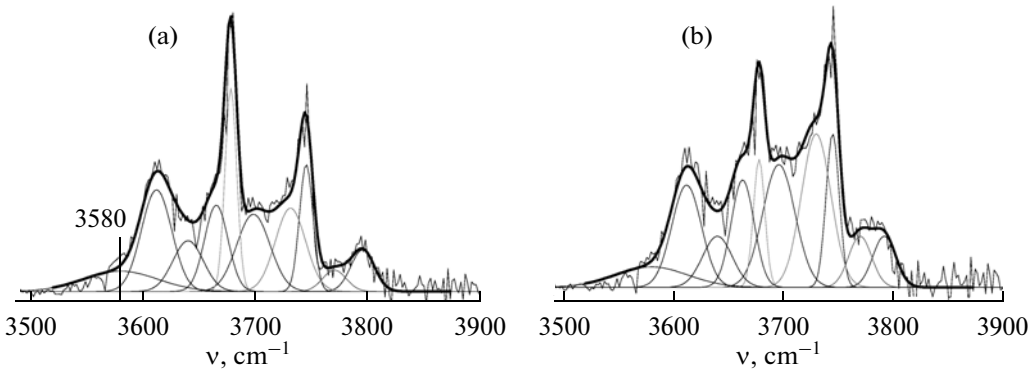

Fig. 3. Decomposition of the IR spectra of supports (*1*) AZ-1 and (*2*) AZ-2 into individual components in the region of hydroxyl groups.

[11]. Note that the concentrations of the above OH groups on the surfaces of the test supports were similar (Table 2); at the same time, the total concentration of hydroxyl groups on the surface of AZ-1 was found lower than that on AZ-2.

Figure 4 shows the spectra of CO adsorbed on the test supports in the regions of ν(CO) and hydroxyl groups as the CO pressure was changed from 0.1 to 10 Torr. Upon the interaction of CO with OH groups, a decrease in the intensity of absorption bands due to hydroxyl groups was observed (they appear as minimums in the spectrum) with the simultaneous appearance of wide absorption bands in the region of 3200–3600 cm^{-1}, which belong to hydrogen-bonded OH groups (Figs. 4c, 4d). According to Paukshtis [11], a wide absorption band at 3282 cm^{-1} indicates the presence of BASs; in this case, a band at 3612 cm^{-1} shifted by 330 cm^{-1}. The shift characterizes the strength of a proton-donor center, and it is close to the values observed in zeolite HZSM-5 [11]. The surface concentrations of BASs evaluated from the integrated intensity of an absorption band at 3282 cm^{-1} on test supports AZ-1 and AZ-2 were similar: 46 and 51 μmol/g, respectively.

An absorption band in the region of ν(CO) = 2142 cm^{-1} belongs to the physically adsorbed CO (Figs. 4a, 4b). An intense absorption band at 2158 cm^{-1}, which was observed at a CO pressure of 10 Torr, was due to the formation of CO complexes with OH groups through weak hydrogen bonds. Absorption bands at 2173–2178 cm^{-1} belong to CO molecules adsorbed at BASs.

In addition to BASs, the test supports contain four types of LASs, which correspond to absorption bands at 2187–2192, 2202, 2220, and 2232 cm^{-1} (Figs. 4a, 4b). The surface concentrations of these LASs are different (Table 3), and this difference is most significant for weak LASs (absorption bands at 2187–2192 cm^{-1}). The total concentration of LASs per 1 m^2 on support AZ-1 is lower than that on AZ-2 by a factor of about 3 (Table 3).

Thus, synthesized supports AZ-1 and AZ-2, which have the same composition but differ in preparation procedures, are characterized by not only different textures but also different surface acidities, which can exert an effect on both the dispersity and distribution of an active component and the properties of the resulting catalysts in the cracking reaction.

Characteristics of the Catalysts

The preliminary study of the oxide precursors of the catalysts performed using X-ray diffraction (XRD) analysis showed that the active components occurred in a highly dispersed state, and they were not identified by XRD analysis. The properties of the sulfidized catalysts were studied after their testing in the reaction of VGO hydrocracking.

Catalyst characterization by high-resolution transmission electron microscopy (HRTEM). According to

Table 2. Positions of absorption band maximums due to OH groups and the concentrations of these groups on the support surfaces

Sample	ν(OH), cm^{-1}									Σ[OH], μmol/g
	3612	3640	3665	3678	3700	3730	3745	3770	3790	
AZ-1	75	37	49	58	62	61	42	12	42	438
AZ-2	75	37	61	36	98	112	50	29	29	527

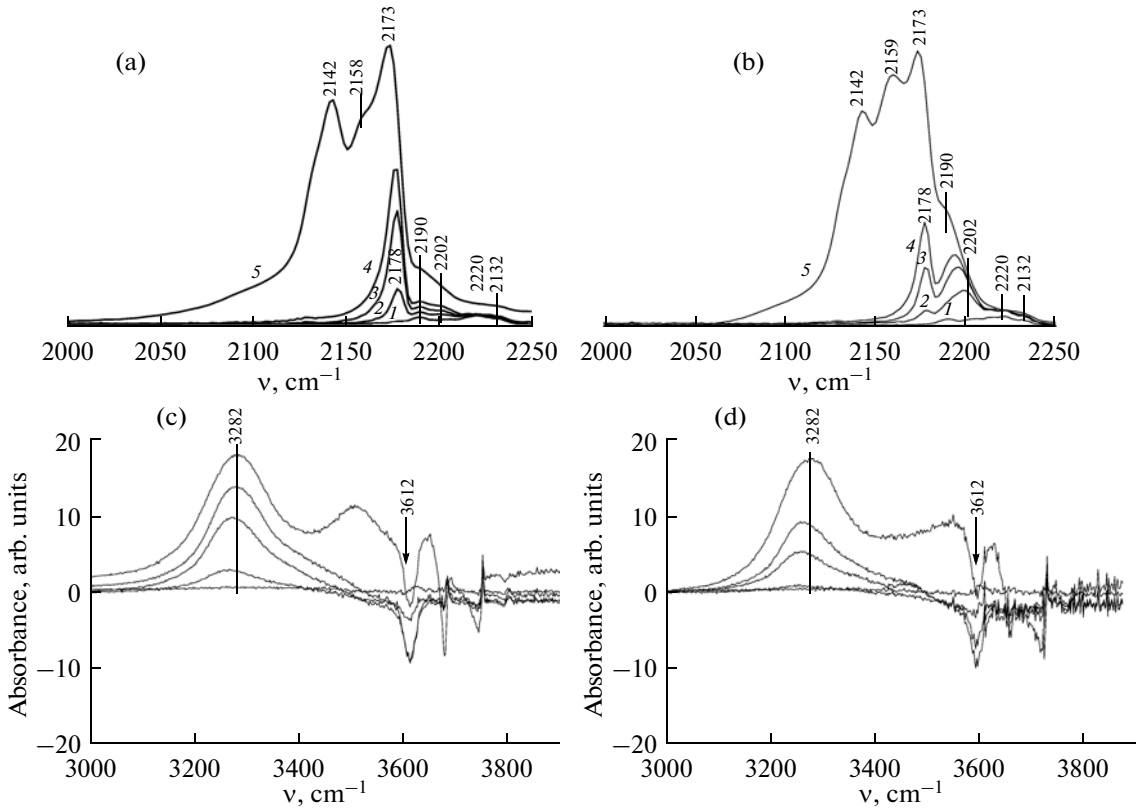

Fig. 4. IR spectra of CO adsorbed on supports (a, c) AZ-1 and (b, d) AZ-2 at the following pressures, Torr: (*1*) 0.1, (*2*) 0.4, (*3*) 1.0, (*4*) 1.5, and (5) to 10. The regions of (a, b) ν(CO) and (c, d) hydroxyl groups.

HRTEM data, the components of the support—zeolite (Figs. 5a, 5b) and aluminum oxide (Figs. 5a, 5c)—were different in morphology: β zeolite consisted of particles with a size of ~1 μm with a well-pronounced crystalline channel structure (Fig. 5d); Al_2O_3 had a block (mesoporous) morphology and consisted of agglomerated partially coalesced isometric crystallites with a characteristic size of ~7 nm (Fig. 5d).

An active component in the form of laminar Ni–W–S sulfide species was mainly located on the surface of Al_2O_3 with the adjoining of layers to the faces of support particles; on β zeolite, Ni–W–S sulfide particles were observed rarely only in the cases they were in contact with the individual particles of Al_2O_3 located on zeolite (Fig. 5d). The Ni–W–S sulfide particles had a length of 7–8 nm and a thickness from 1 to 10–13 monolayers (Fig. 6). The catalysts in question were characterized by identical structures and distributions of the Ni–W–S active component over the support surface; the basic difference between the catalysts consists in the thickness of Ni–W–S sulfide species. It is evident that multilayer (to 10 monolayers) Ni–W–S species were formed on the surface of catalysts Ni–W/AZ-1(a) (Fig. 6a) and Ni–W/AZ-1(b) (Fig. 6b), whereas single-layer Ni–W–S species were mainly observed on the surface of catalysts Ni–W/AZ-2(a) (Fig. 6c) and Ni–W/AZ-2(a*) (Fig. 6d). Furthermore, upon the supporting of an active component with the use of a complex-forming agent (citric acid), tungsten oxide particles (Fig. 7), which were sulfidized only at the external surface, were also present in a small amount on the surface of catalyst Ni–W/AZ-2(a*). Thus, the use of a support with a high specific surface

Table 3. Positions of absorption band maximums due to CO and concentrations on the support surfaces

Support	ν(CO), cm^{-1}				Σ[LAS], μmol/g (μmol/m^2)
	2187–2192	2202	2220	2232	
AZ-1	58	12.6	5.6	4.8	81 (0.37)
AZ-2	395	20	16.5	7.5	439 (1.16)

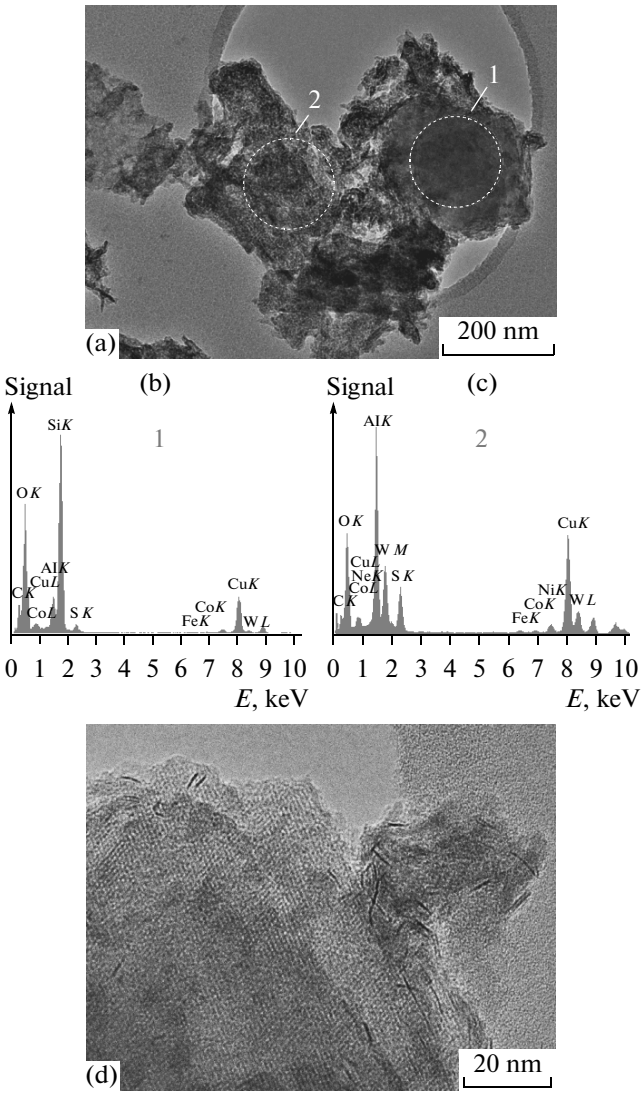

Fig. 5. (a) TEM and (d) HRTEM micrographs and (b, c) the EDX spectra measured in the regions (1 and 2) marked in the TEM micrograph for a Ni–W catalyst after testing in the reaction of VGO hydrocracking.

area (AZ-2) facilitated the formation of highly dispersed single-layer Ni–W–S species.

Catalyst characterization by X-ray photoelectron spectroscopy (XPS). Preliminary analysis of a typical survey XPS spectrum of sample Ni–W/AZ-1(a) showed that it contained peaks characteristic of tungsten, aluminum, silicon, sulfur, carbon, oxygen, and nickel; the impurities of other elements were not detected within the accuracy of XPS analysis. A comparison of the binding energies obtained from the positions of peaks due to the base elements (Al2*p*), (Al2*s*), (S2*p*), (C1*s*), and (O1*s*), which were present in the test samples, in the XPS spectrum suggests that they are 74.7, 119.6, 162.3, 284.8, and 531.8 eV, respectively, regardless of the nature of the catalyst.

Tungsten in the test samples occurred as a sulfide ($E_b = 32.6$ eV) and oxide with the predominance of the former, as evidenced by a comparison of the W4$f_{7/2}$ XPS spectra of the test samples and the XPS spectra of WS_2 and WO_3 (Fig. 8) [16–21]. For comparison and more correct identification of the chemical state of tungsten in the samples and for the determination of a ratio between its sulfide (W_s) and oxide species (W_{ox}), the spectra of the W4$f_{7/2}$ level were normalized to the intensity of a peak with E_b = 32.6 eV (Fig. 9), and peaks in the region of W4$f_{7/2}$ were separated into individual spectral components using the XPS-Peak software. According to the results obtained (Fig. 10a, Table 4), the W_{ox}/W_s ratio varied within the range of 0.32–0.42; in this case, the fraction of the oxide species increased in the order Ni–W/AZ-1(a) → Ni–W/AZ-2(a) → Ni–W/AZ-1(b) → Ni–W/AZ-2(a*). The degree of tungsten sulfidation W_s/W_{tot}, which was determined as the ratio of the area of the sulfide species to the total peak area of W4$f_{7/2}$, was 0.71–0.76; that is, for the catalysts in question, it decreased in the order Ni–W/AZ-1(a) → Ni–W/AZ-2(a) → Ni–W/AZ-1 (b) → Ni–W/AZ-2(a*).

Figure 10b shows the Ni2$p_{3/2}$ spectra of the test samples; it can be seen that two peaks with $E_b = 854.0 \pm 0.1$ and 856.7 ± 0.1 eV were present at the Ni2$p_{3/2}$ line. The former peak can be assigned to nickel atoms in a sulfide environment, and the latter, to nickel atoms in an oxygen environment (for example, as $NiSO_4$, possibly, as a result of oxidation in air after the reaction, or $NiAl_2O_4$) [17–21]. For determining the ratio between the sulfide and oxide nickel components, we decomposed the Ni2$p_{3/2}$ line into individual spectral components, as in the case of tungsten. It can be seen (Table 4) that the Ni_{ox}/Ni_s ratio increased in the order Ni–W/AZ-1(a) → Ni–W/AZ-2(a) → Ni–W/AZ-2(a*) → Ni–W/AZ-1(b); that is, in a somewhat different sequence than that in the case of W_{ox}/W_s.

A special feature of the test samples is that, according to XPS data, the Ni : W surface atomic ratios were different (Table 4), although, according to the results of chemical analysis, the samples had the same concentrations of active components and their atomic ratio was 0.7. We found that the Ni : W atomic ratio in near-surface layers coincided with the bulk ratio only for Ni–W/AZ-2(a), whereas it was lower than the bulk ratio for catalysts Ni–W/AZ-1(a) and Ni–W/AZ-2(a*) or higher than the bulk ratio for Ni–W/AZ-1(b) (Table 4). Consequently, the surface became enriched in nickel upon the sequential supporting of an active component onto the support; this did not exclude the formation of surface nickel aluminates. Indeed, the Ni : Al surface atomic ratio only in this catalyst was higher that that in the other samples (Table 4).

In the S2*p* spectra (Fig. 11) of the test samples, two peaks with E_b = 162.2 and 169.2 eV were observed,

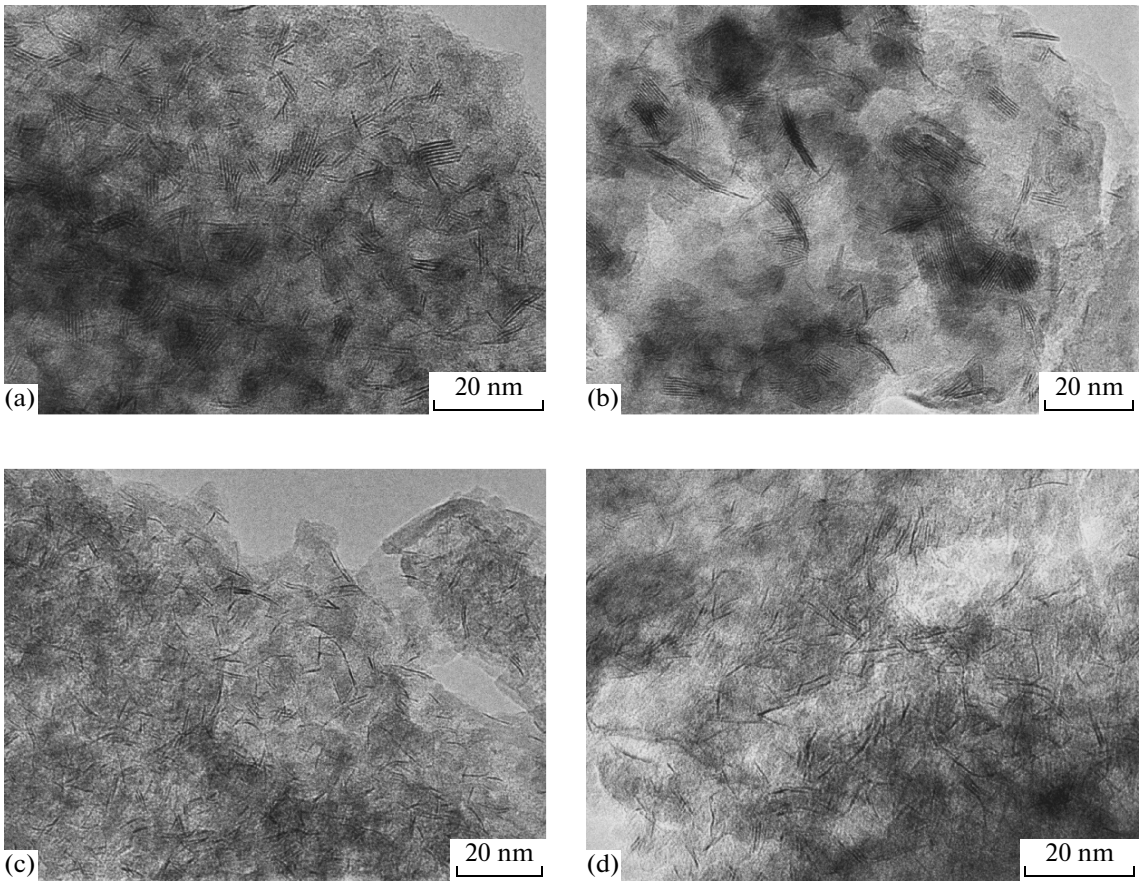

Fig. 6. HRTEM micrographs of the catalysts: (a) Ni–W/AZ-1(a), (b) Ni–W/AZ-1(b), (c) Ni–W/AZ-2(a), and (d) Ni–W/AZ-2(a*).

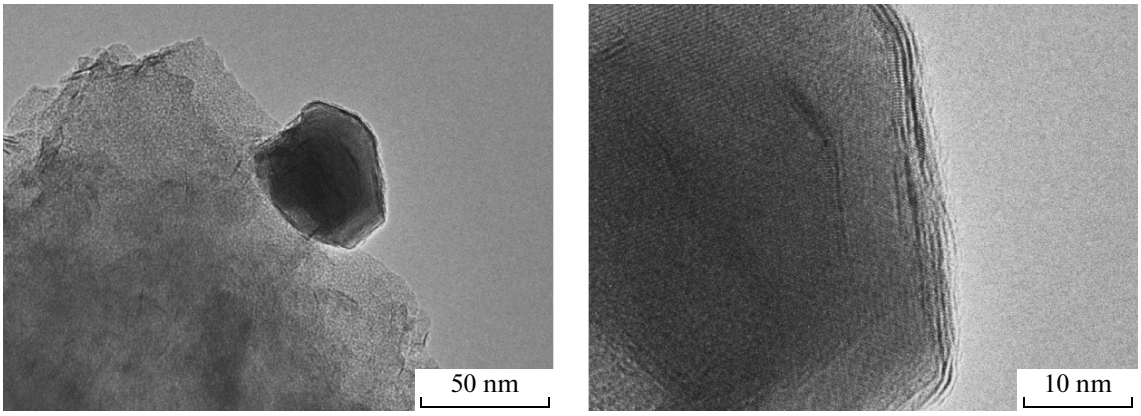

Fig. 7. HRTEM micrographs of Ni–W/AZ-2(a*): a tungsten oxide particle sulfidized at the outer surface.

which are characteristic of sulfides (S^{2-}) and sulfate ions (SO_4^{2-}), respectively [22–25]; the latter can occur as $Al_2(SO_4)_3$. In the test samples, the ratio between sulfate (S_t is sulfate) and sulfide (S_d is sulfide) states changed, and it increased in the following order depending on the nature of the support and the method of supporting the active components: Ni–W/AZ-1(a) → Ni–W/AZ-2(a) → Ni–W/AZ-2(a*) → Ni–W/AZ-1(b). That is, catalyst Ni–W/AZ-1(b),

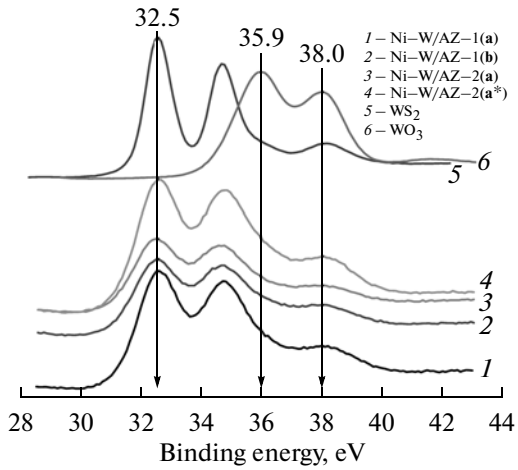

Fig. 8. XPS spectra of the W $4f_{7/2}$ level of the catalysts.

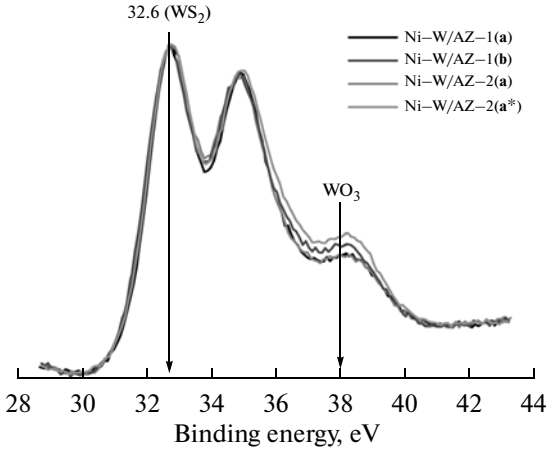

Fig. 9. XPS spectra of the W $4f_{7/2}$ level normalized to the peak intensity of the tungsten sulfide species (E_b = 32.6 eV).

which was obtained by the sequential supporting of active components onto the support, was sulfidized to a lesser degree. Thus, the preparation of catalysts by the impregnation of a support with a mixed solution of active components resulted in the greatest degree of its sulfidation and a smaller fraction of active components, which occurred in an oxidized state.

Activity of the catalysts. It is well known that the hydrocracking of VGO changes its fractional composition because of cracking reactions and leads to the formation of motor fuels (gasoline and/or diesel fuel fractions) with the simultaneous removal of sulfur, nitrogen, oxygen, and metals from the starting material. The fractional composition of the products obtained in the presence of the catalysts was determined by simulated distillation. According to the experimental results (Table 5), the conversion of VGO varied from 30 to 70% and depended on both the nature of the catalyst and the temperature of hydrocracking (T_r). In this case, gas (C_1–C_4), C_5 gasoline (185°C), and diesel fuel (185–360°C) were formed. Diesel fuel was the main product because the yields of gas and gasoline varied in the ranges of 1.6–7.5 and 5.4–22 wt %, respectively.

In accordance with data published by Eijsbouts et al. [5], the BASs caused by the presence of zeolite determine the activity of catalysts in hydrocracking reactions. The catalysts contain the same zeolite amount. Taking into account that Ni–W–S sulfide species are mainly distributed on aluminum oxide, we can assume that the concentrations of BASs observed on supports AZ-1 and AZ-2, which were 46 and 51 μmol/g, respectively, did not change significantly after supporting an active component. Thus, because of similar BAS concentrations in the catalysts (changes within the limits of experimental error), differences in their cracking activity are not so significant (Table 5). However, according to Zhang et al. [26], not only BASs but also LASs and their strength distribution play a determining role in the reactions of hydrocracking. Indeed, it can be seen (Table 5) that the selectivity for gasoline is higher on the catalysts prepared based on AZ-2, as compared with the catalysts prepared on support AZ-1. Taking into account that the surface concentration of LASs, in particular, weak LASs, on AZ-2 is higher than that on AZ-1 by a factor of about 3, we assume that the presence of a high concentration of weak LASs (Table 3) on the surface of catalysts Ni–W/AZ-2 is responsible for the increased selectivity for gasoline. A smaller concentration of weak LASs and a greater average pore diameter of catalysts prepared on AZ-1 (Table 1) contributed to an increase in the selectivity for diesel fuel and facilitated the diffusion of the large molecules of both the initial reagents and the reaction products; this is consistent with published data [26].

The selectivity for diesel fuel on the test samples decreased with conversion (Fig. 12a); in this case, Ni–W/AZ-1(a) was the most selective catalyst all other factors being the same. The yield of diesel fuel increased with conversion (Fig. 12b) to reach 41 wt %. In this case, Ni–W/AZ-1(a) was also a more effective catalyst. In the region of low conversions, it was almost no difference between the test samples, whereas this difference increased in the region of high conversions. Catalyst Ni–W/AZ-2(a*), which was obtained with the use of a complex-forming component in the supporting of an active component onto the support, was found less effective in the reaction of VGO hydrocracking. First, the above catalysts are different in the morphology of Ni–W–S sulfide particles: multilayer species were observed on the surface of Ni–W/AZ-1(a) and practically single-layer ones, on Ni–W/AZ-2(a*). Second, according to XPS data, the degree of tungsten sulfidation decreased in the order Ni–W/AZ-1(a) ≈ Ni–W/AZ-2(a) > Ni–W/AZ-1(b) ≈ Ni–W/AZ-2(a*).

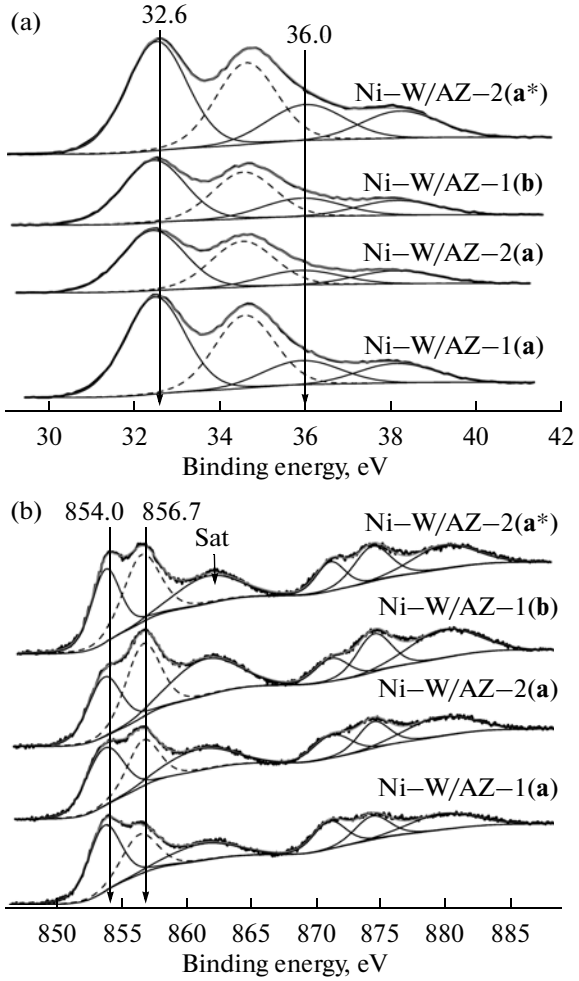

Fig. 10. XPS spectra of the (a) W $4f_{7/2}$ and (b) Ni $2p_{3/2}$ levels of the catalysts after deconvolution into individual spectral components.

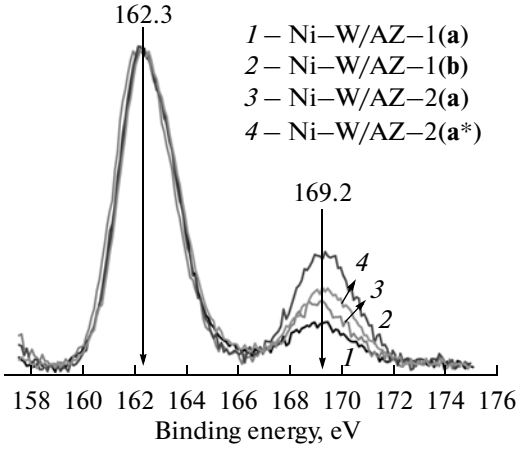

Fig. 11. XPS spectra of the S $2p$ level of the catalysts.

Consequently, the catalyst characterized by a higher degree of sulfidation and containing multilayer Ni–W–S sulfide species on the surface provided a higher yield of diesel fuel upon the hydrocracking of VGO.

The catalysts behaved in a different manner in the reactions of VGO hydrodesulfurization and hydrodenitration. It can be seen (Table 6) that, in the presence of catalysts obtained on support AZ-1, the residual sulfur and nitrogen concentrations at 380°C were 1220–1300 ppm of S and 411–415 ppm of N, and those for catalysts obtained on support AZ-2 were lower by factors of about 2 and 1.5, respectively. An increase in T_r facilitated a decrease in the residual sulfur and nitrogen concentrations; however, the tendency determined by the nature of the catalyst was retained (Table 6). The experimental results show that the high specific surface area of support AZ-2 leads to a higher dispersion of the active component (predominantly, single-layer Ni–W–S sulfide species were present), which determines the increased activity in the reactions of VGO hydrodesulfurization and hydrodenitration. In this case, the supporting of an active component on support AZ-2 in the presence of a complex-forming agent makes it possible to additionally increase the hydrodesulfurizing and hydrodenitrating activity of catalyst Ni–W/AZ-2(a*) (Table 6).

We found that supports AZ-1 and AZ-2, which differ in both texture characteristics and the surface concentrations of BASs and LASs, were obtained upon changing the method of mixing aluminum oxide and β zeolite at the same concentrations. Correspondingly, the formation of active components in the sulfidized Ni–W-containing catalysts occurred differently on

Table 4. Atomic concentrations of the elements in the catalysts, as determined by XPS

Catalyst	Ni/W	W/Al	Ni/Al	O/Al	S/Al	W_{ox}/W_s	W_s/W_{tot}	Ni_{ox}/Ni_s	Ni_s/Ni_{tot}	S_t/S_d
Ni–W/AZ-1(**a**)	0.46	0.055	0.03	2.04	0.15	0.32	0.76	0.69	0.59	0.12
Ni–W/AZ-1(**b**)	0.84	0.051	0.04	2.80	0.16	0.38	0.72	1.36	0.42	0.39
Ni–W/AZ-2(**a**)	0.70	0.043	0.03	2.68	0.13	0.33	0.75	0.85	0.54	0.19
Ni–W/AZ-2(**a***)	0.51	0.061	0.03	2.16	0.17	0.42	0.71	1.29	0.44	0.22

Note: W_s and Ni_s or W_{ox} and Ni_{ox} are the sulfide or oxide W and Ni species, respectively; W_{tot} and Ni_{tot} are the total areas of XPS spectra for Ni $2p_{3/2}$, without the satellite taken into account (Sat in Fig. 10b); S_t is sulfate; and S_d is sulfide.

Table 5. Yields of hydrocracking products depending on the reaction temperature in the presence of the catalysts

Catalyst	T_r, °C	X, %	Yield, wt %				Selectivity, wt %		
			Gas (C_1–C_4)	Gasoline C_5 (185°C)	Diesel fuel (185–360°C)	Residue (>360°C)	Gas (C_1–C_4)	Gasoline C_5 (185°C)	Diesel fuel (185–360°C)
Ni–W/AZ-1(**a**)	380	30.3	1.7	5.5	23.1	69.7	5.4	18.2	76.3
	390	36.5	2.3	6.6	27.6	63.5	6.2	18.2	75.6
	400	48.2	3.2	9.7	35.4	51.8	6.6	20.0	73.3
	410	64.8	6.6	17.4	40.8	35.2	10.1	26.9	63.0
Ni–W/AZ-2(**a**)	380	30.3	1.6	5.4	23.4	69.7	5.1	17.9	77.0
	390	37.1	2.5	7.1	27.6	62.9	6.6	19.1	74.3
	400	48.5	3.6	10.4	34.6	51.5	7.3	21.5	71.2
	410	67.6	6.9	19.8	41.0	32.4	10.1	29.3	60.6
Ni–W/AZ-1(**b**)	380	30.3	1.6	5.5	23.2	69.7	5.3	18.1	76.7
	390	38.3	2.6	7.2	28.6	61.7	6.7	18.8	74.5
	400	47.4	3.8	9.9	33.7	52.6	7.9	21.0	71.1
	410	64.6	6.8	17.6	40.2	35.4	10.5	27.3	62.2
Ni–W/AZ-1(**a***)	380	32.4	1.8	6.0	24.6	67.6	5.4	18.5	76.1
	390	38.1	2.5	7.6	28.1	61.9	6.4	19.9	73.4
	400	48.9	3.7	10.8	34.5	51.1	7.5	22.0	70.5
	410	70.4	7.5	22.1	40.8	29.6	10.7	31.3	58.0

Table 6. Residual sulfur and nitrogen concentrations in hydrocracking products

Catalyst	Concentrations of S and N, ppm							
	S	N	S	N	S	N	S	N
	Temperature, °C							
	380		390		400		410	
Ni–W/AZ-1(**a**)	1300	415	680	273	270	109	150	24
Ni–W/AZ-1(**b**)	1220	411	621	270	310	142	178	61
Ni–W/AZ-2(**a**)	800	322	380	209	150	84	77	25
Ni–W/AZ-2(**a***)	638	297	350	188	137	69	85	25

Note: Conditions: space velocity, 1 h^{-1}; H_2 to feed ratio, 1000; pressure, 10 MPa.

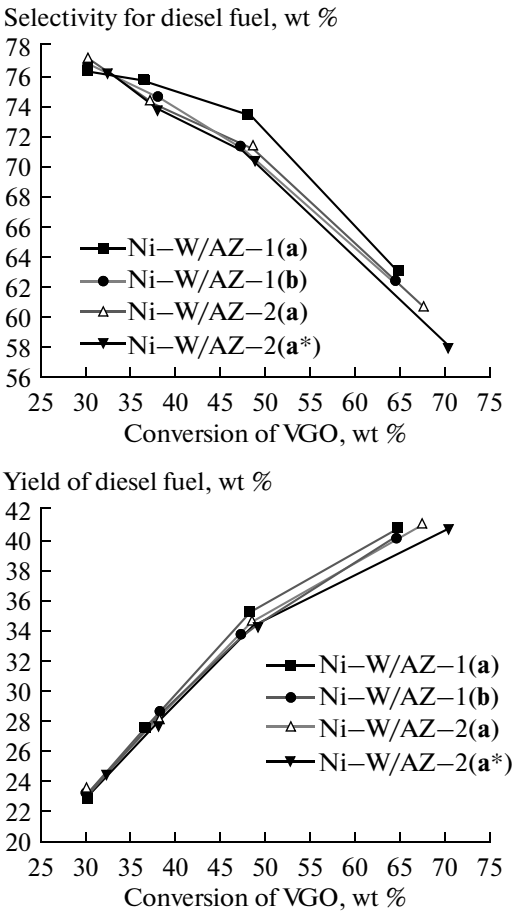

Fig. 12. Dependence of (a) selectivity and (b) the yield of diesel fuel on the conversion of VGO.

different supports. Support AZ-2, whose specific surface area is 380 m^2/g, facilitated the formation of highly dispersed mainly single-layer N–W–S sulfide species, whereas multilayer sulfide species were formed on the surface of AZ-1.

Different surface acidities of supports and methods of supporting the active components of catalysts lead to different distributions of the active component and different degrees of its sulfidation. This clearly manifested itself upon a comparison of two catalysts Ni–W/AZ-1(a) and Ni–W/AZ-2(a), which differ in the supports. According to XPS data, the Ni : W atomic ratio in the near-surface layers of catalyst Ni–W/AZ-2(a) is comparable with the bulk ratio, and it is lower on Ni–W/AZ-1(a); that is, the surface of this catalyst is depleted of nickel. Consequently, the increased concentration of LASs on the surface of support AZ-2 minimizes the interaction of the support with the active components. Correspondingly, it provides the more complete interaction between Ni- and W-containing components, which determines close Ni : W atomic ratios both on the surface and in the bulk. At the smaller surface concentration of LASs of support AZ-1, the partial interaction of active components with the support becomes possible to change the Ni : W surface atomic ratio. On going from the combined impregnation of a support with a solution of active component salts to the sequential impregnation, the surface of catalyst Ni–W/AZ-1(b) became enriched in nickel; this was likely due to the formation of surface nickel aluminates. The above changes can result in different degrees of sulfidation, which were observed experimentally. Indeed, the greatest degree of sulfidation was reached on samples Ni–W/AZ-1(a) and Ni–W/AZ-2(a), whereas the smallest degree was reached on Ni–W/AZ-1(b).

The above differences in the catalysts caused their different behaviors in the reactions of VGO cracking, hydrodesulfurization, and hydrodenitration. We found that the yield of liquid products in the reaction of VGO hydrocracking at $T_r = 410°C$ decreases in the order Ni–W/AZ-1(a) → Ni–W/AZ-2(a) → Ni–W/AZ-1(b) → Ni–W/AZ-2(a*). Catalyst Ni–W/AZ-1(a) was the most selective for diesel fuel. On the contrary, the hydrodesulfurization and hydrodenitration of VGO occurred most effectively on catalyst Ni–W/AZ-2(a*).

REFERENCES

1. Kapustin, V.M., *Toplivno-energeticheskii kompleks Rossii: Sbornik materialov VII Mezhdunarodnogo foruma* (Energy Economy of Russia: Proc. VII Int. Conf.), St. Petersburg, 2007, p. 112.
2. Kapustin, V.M. and Gureev, A.A., *Tekhnologiya pererabotki nefti. Destruktivnye protsessy* (Petroleum Refining Technology: Destruction Processes), Moscow: Kolos, 2007.
3. Camblor, M.A., Corma, A., Martinez, A., Martinez-Soria, V., and Valencia, S., *J. Catal.*, 1998, vol. 179, p. 537.
4. Ali, M.A., Kimura, T., Suzuki, Y., Al-Saleh, M.A., Hamid, H., and Inui, T., *Appl. Catal., A*, 2002, vol. 277, p. 63.
5. Eijsbouts, S., Mayo, S.W., and Fujita, K., *Appl. Catal., A*, 2007, vol. 322, p. 58.
6. Reiche, M.A., Maciejewski, M., and Baiker, A., *Catal. Today*, 2000, vol. 56, p. 347.
7. Bataille, F., Lemberton, J.L., Perot, G., Leyrit, P., Cseri, T., Marchal, N., and Kasztelan, S., *Appl. Catal., A*, 2001, vol. 220, p. 191.
8. Corma, A., Fornes, V., Monton, J.B., and Orchilles, A.V., *J. Catal.*, 1987, vol. 107, p. 288.
9. Ali, M.A., Tasumi, T., and Masuda, T., *Appl. Catal., A*, 2002, vol. 233, p. 77.
10. Serwicka, E.M., *Catal. Today*, 2000, vol. 56, p. 335.
11. Paukshtis, E.A., *Infrakrasnaya spektroskopiya v geterogennom kislotno-osnovnom katalize* (Infrared Spectroscopy in Heterogeneous Acid–Base Catalysis), Novosibirsk: Nauka, 1992.
12. Price, W., *Analytical Atomic Absorption Spectroscopy*, New York: Wiley-Interscience, 1972.

13. Scofield, J.H., *J. Electron Spectrosc. Relat. Phenom.*, 1976, vol. 8, p. 129.
14. Grigor'ev, Ya.M., Pozdnyakov, D.V., and Filimonov, V.N., *Zh. Fiz. Khim.*, 1972, vol. 46, p. 316.
15. Davydov, A.A., Shepotko, M.L., and Budneva, A.A., *Catal. Today*, 1995, vol. 24, p. 225.
16. Sun, M., Burgi, T., Cattaneo, R., and Prins, R., *J. Catal.*, 2001, vol. 197, p. 172.
17. Breysse, M., Cattenot, M., Decamp, T., Frety, R., Gachet, C., Lacroix, M., Leclercq, C., de Mourgues, L., Portefaix, J.L., Vrinat, M., Houari, M., Grimblot, J., Kasztelan, S., Bonnelle, J.P., Housni, S., Bachelier, J., and Duchet, J.C., *Catal. Today*, 1988, vol. 4, p. 39.
18. Reinhoudt, H.R., Crezee, E., van Langeveld, A.D., Kooyman, P.J., van Veen, J.A.R., and Moulijn, J.A., *J. Catal.*, 2000, vol. 196, p. 315.
19. Vissenberg, M.J., van der Meer, Y., Hensen, E.J.M., de Beer, V.H.J., van der Kraan, A.M., van Santen, R.A., and van Veen, J.A.R., *J. Catal.*, 2001, vol. 198, p. 151.
20. Sun, M., Burgi, T., Cattaneo, R., van Langeveld, D., and Prins, R., *J. Catal.*, 2001, vol. 201, p. 258.
21. Zuo, D., Vrinat, M., Nie, H., Maugec, F., Shi, Y., Lacroix, M., and Li, D., *Catal. Today,* 2004, vol. 93–95, p. 751.
22. Legrand, D., Nesbitt, H.W., and Bancroft, G.M., *Am. Mineral.*, 1998, vol. 83, p. 1256.
23. Startsev, A.N., Kalinkin, A.V., Zakharov, I.I., Aksenov, D.G., and Parmon, V.N., *J. Mol. Catal. A: Chem.*, 2000, vol. 151, p. 171.
24. Blanchard, L., Grimblot, J., and Bonnelle, J.P., *J. Catal.,* 1986, vol. 98, p. 229.
25. Rodriguez-Castellon, E., Jimenez-Lopez, A., and Eliche-Quesada, D., *Fuel*, 2008, vol. 87, p. 1195.
26. Zhang, X., Guo, Q., Qin, B., Zhang, Z., Ling, F., Sun, W., and Li, R., *Catal. Today*, 2010, vol. 149, p. 212.